ACS APPLIED MATERIALS & INTERFACES

Research Article

www.acsami.org

Facile Synthesis and High Anode Performance of Carbon Fiber-Interwoven Amorphous Nano-SiO_x/Graphene for Rechargeable Lithium Batteries

Dan Thien Nguyen,[†] Cao Cuong Nguyen,[†] Jong-Seon Kim,[†] Je Young Kim,[‡] and Seung-Wan Song*[,†]

[†]Department of Fine Chemical Engineering & Applied Chemistry, Chungnam National University, Daejeon 305-764, Republic of Korea

[‡]Battery R&D, LG Chem, Ltd., Daejeon 305-380, Republic of Korea

ABSTRACT: We present the first report on carbon fiber-interwoven amorphous nano-SiO_x/graphene prepared by a simple and facile room temperature synthesis of amorphous SiO_x nanoparticles using silica, followed by their homogeneous dispersion with graphene nanosheets and carbon fibers in room temperature aqueous solution. Transmission and scanning electron microscopic imaging reveal that amorphous SiO_x primary nanoparticles are 20−30 nm in diameter and carbon fibers are interwoven throughout the secondary particles of 200−300 nm, connecting SiO_x nanoparticles and graphene nanosheets. Carbon fiber-interwoven nano-$SiO_{0.37}$/graphene electrode exhibits impressive cycling performance and rate-capability up to 5C when evaluated as a rechargeable lithium battery anode, delivering discharge capacities of 1579−1263 $mAhg^{-1}$ at the C/5 rate with capacity retention of 80% and Coulombic efficiencies of 99% over 50 cycles, and nearly sustained microstructure. The cycling performance is attributed to synergetic effects of amorphous nano-SiO_x, strain-tolerant robust microstructure with maintained particle connectivity and enhanced electrical conductivity.

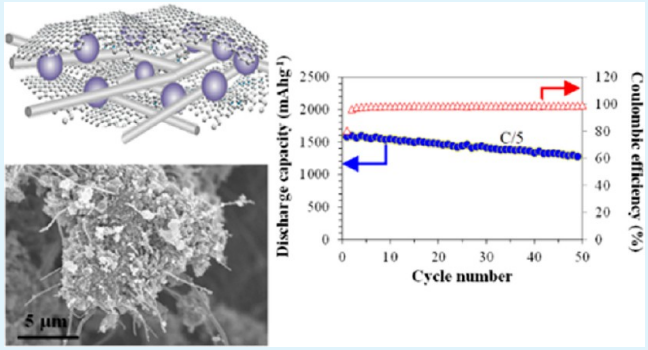

KEYWORDS: *rechargeable lithium batteries, anode, amorphous silicon suboxide, graphene, carbon fiber*

INTRODUCTION

Carbon composites of silicon (Si) and silicon monoxide (SiO) are considered as alternative anode materials to graphite for rechargeable lithium batteries, due to the high theoretical capacity of 3579 $mAhg^{-1}$ for Si at room temperature and safer operation voltage above lithium.[1,2] Si, however, suffers from capacity fade due to large volume change upon lithiation and delithiation during cycling. SiO is favored with respect to cycling stability despite sacrificing the capacity, as lithium oxide (Li_2O) and lithium silicates formed during initial lithiation better accommodates significant volume change of Si.[3,4]

This study focuses on silicon suboxide (SiO_x) nanoparticles for attaining stabilized electrode performance. For the SiO_x with higher fraction of oxygen ($x > 0.5$), while the effect of strain buffering increases, the resistivity increases, which deleteriously affects electron transport kinetics.[5,6] Crystallinity is another factor influencing cycling ability; amorphous Si and SiO_x cycle better than crystalline counterparts, because of the absence of two-phase regions during formation of various lithiated alloys.[7,8] The rational design and synthesis of carbon composite of amorphous SiO_x ($x < 0.5$) nanoparticles, which allows a short lithium diffusion path but accommodates volume change by the presence of oxygen, are highly desirable to solve the issues with Si.

Development of preparation method of Si-based carbon composites was extensively studied, in a manner most of which included the physical mixing of commercial crystalline Si or SiO powders with carbon (e.g., graphite), or surface carbon-coating using organic sources.[9−13] Nanostructured or porous Si enabled to show excellent electrochemical properties,[14−16] but there was a trade-off with complicated and expensive synthetic procedures. Solution-based synthesis would be suitable for scalable production but elevated reaction temperature produced crystalline Si.[17,18] For the source of Si, earth-abundant silica (SiO_2) would be the most efficient choice. Recent studies of magnesioreduction of silica to crystalline Si used the magnesium vapor onto porous silica at 650 °C.[19] The use of higher cost SiO was attempted by mechanochemical reduction with lithium metal and vacuum heating at 500 °C.[20] Heat treatment at high temperature produced crystalline micro- or macro-Si that exhibited a limited cycling performance. Synthesis of SiO_x is however rarely reported. Here, we focus on a room temperature (RT) facile synthesis to amorphous nano-SiO_x, using silica and lithium.

Received: August 19, 2013
Accepted: October 10, 2013
Published: October 10, 2013

Scheme 1. Facile Room Temperature Synthesis of Homogeneously Dispersed Carbon Fiber-Interwoven Amorphous Nano-SiO_x/Graphene

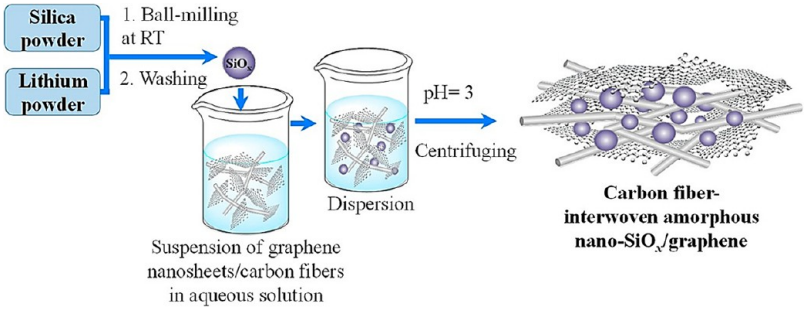

Graphene is an attractive carbon component for preparing the carbon composite of SiO_x due to its high electrical conductivity and flexible characteristics. Earlier studies for graphene composites used the mixing of Si or SiO with graphene oxide followed by thermal reduction (700 °C) or vapor deposition (500 °C) of nano-Si on graphene and carbon-deposition, where Si (or SiO) is fully encapsulated by graphene nanosheets.[21−24] They exhibited improved cycling performance than Si only and Si-graphite but an improvement of synthetic procedure for performance enhancement and scalable production remains. Although a fully encapsulated nanostructure is favorable for electrical conductivity, electrolyte-wetting and lithium transport might not be easy. We employ carbon fiber as a pillar that supports graphene nanosheets forming the open spaces between the nanosheets, and permits an easy electrolyte-wetting through the open spaces. Additionally, carbon fiber enhances electrical conductivity. Obtaining the homogeneous dispersion of SiO_x in graphene matrix is a critical point of synthetic technique, because cycling performance is strongly dependent on the dispersion ability of each component.[21−24] However, nonwettability of carbon fiber in water due to hydrophobic surface limits its use in composite applications.[25] In this work, this dispersion problem is overcome by a simple surface functionalization.

Herein, we present the first report of carbon fiber-interwoven nano-SiO_x/graphene as a high-performance anode material for rechargeable lithium batteries, which is prepared by a simple and facile RT synthesis.

EXPERIMENTAL SECTION

Synthesis. Preparation of carbon fiber-interwoven amorphous nano-SiO_x/graphene started from synthesizing first the SiO_x nanoparticles via a simple single displacement reaction of oxygen from silica to lithium metal, as illustrated in Scheme 1 and eq 1. Lithium powder (20−30 μm, SLMP, FMC) and silica nanopowder (10−20 nm, 99.5%, Aldrich) were mixed in a 4:1 molar ratio and ground thoroughly in a mortar for 30 min in Ar-filled glovebox. The mixed powders were transferred to a bowl of vibrational ball-miller (Mini-mill Pulverisette 23, Fritsch) and milled at the oscillation frequency of 50 Hz for 3h at RT. The ball-milled powders were moved to the 0.5 M HCl aqueous solution in order to remove Li_2O and/or residual lithium, by which they were converted to LiCl and washed out by water (Li_2O + 2HCl → 2LiCl + H_2O). The resultant powders were separated from the solution using a centrifuge and was washed with a mixed solution of acetone and 1 M HCl (1:1 volume ratio) till pH 7 followed by drying at 30 °C overnight and at 110 °C for 12 h to eliminate water. Finally, black $SiO_{0.37}$ nanoparticles were obtained.

For the preparation of graphene nanosheets, natural graphite powders (Aldrich) were oxidized to graphite oxide (GO) using a modified Hummer's method.[26] To form surface hydroxyl groups at the surface of carbon fibers (100 nm in width, Aldrich) and attain improved dispersion in water, we oxidized carbon fibers in the concentrated HNO_3 acid (63.01%, Junsei) for 5 h. By mixing the carbon fibers and GO powders at an equal weight ratio in RT aqueous solution of 0.5% poly(acrylic acid) (PAA, MW∼1800, Aldrich) and conducting ultrasonication (Jeiotech, UC-05) for 1 h, the suspension of carbon fiber-GO was obtained. PAA served as a stabilizing agent, preventing agglomeration of carbon fibers in water and maintaining the suspension at RT (Figure 1b), and is the same compound to

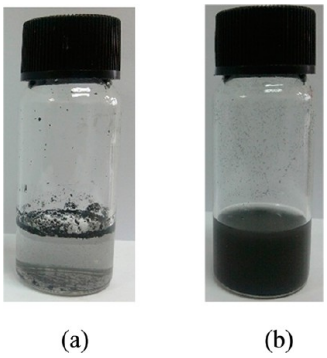

Figure 1. Dispersion ability of surface-oxidized carbon fibers (a) in water only and (b) in 0.5 wt % poly(acrylic acid) aqueous solution. The pictures were taken 3 h after ultrasonication and demonstrate their excellent dispersion ability in poly(acrylic acid) aqueous solution.

binder used in the electrode preparation. For converting the GO to reduced graphene, we added hydrazine hydrate (50−60%, Aldrich) to the suspension of carbon fiber-GO at the ratio of 2 mL of hydrazine hydrate per 1 g of GO.[27] The suspension was stirred at 80 °C for 3 h and finally the suspension of graphene/carbon fiber was obtained. $SiO_{0.37}$ nanoparticles were then added to the RT aqueous suspension of graphene-carbon fibers at the ratio of 80 wt % $SiO_{0.37}$, 10 wt % graphene, and 10 wt % carbon fibers while conducting ultrasonication for 1 h until the suspension of $SiO_{0.37}$/graphene/carbon fiber composite was obtained (Figure 2a). To this suspension, 0.05 M HCl was added slowly to pH 3 until particle agglomeration occurred (Figure 2b). Negative charge of oxygen-containing groups at the surface of graphene nanosheets is neutralized by uptaking the proton from HCl, leading to the agglomeration of graphene nanosheets. Particle agglomeration brings about in situ incorporation of $SiO_{0.37}$ nanoparticles and carbon fibers in between graphene nanosheets (Scheme 1). The $SiO_{0.37}$/graphene/carbon fiber powders were separated from the solution by centrifuging at 1000 rpm and washed with the mixture of water−ethanol (1:1 volume ratio) followed by acetone. Then, resultant composite powders were vacuum-dried at 30 °C for 12 h and at 110 °C for 12 h for the complete removal of water. By the same method, the composite consisting of 80 wt % $SiO_{0.37}$ and 20 wt % graphene was synthesized without the use of carbon fiber for comparison.

Material Characterization. The composition, particle morphology, and crystal structure of synthesized $SiO_{0.37}$ nanoparticles were

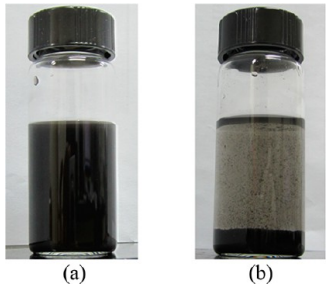

Figure 2. (a) Suspension of nano-$SiO_{0.37}$/graphene/carbon fiber particles in neutral poly(acrylic acid) aqueous solution and (b) the occurrence of particle agglomeration at pH 3.

determined by high-resolution (HR) transmission electron microscopy (TEM, Jeol JEM-2100F) at 200 kV, dispersed selected area electron diffraction (SAED) and energy-dispersive X-ray (EDX) spectroscopy, and powder X-ray diffraction (XRD) measured in 10−80° 2θ at a scan rate of 2°/min at 40 kV and 40 mA using an X-ray diffractometer (Bruker AXS/D8 Discover) with Ni-filtered Cu Kα radiation, respectively. Total carbon content of the composite was confirmed by automatic elemental analyzer (Flash EA1112). Attenuated total reflection (ATR) Fourier transform infrared (FTIR) spectral measurement was conducted using an IR spectrometer (Nicolet 670) with Ge optic and mercury−cadmium−telluride (MCT) detector, where dry nitrogen was purged. IR spectra were collected with 128 scans and spectral resolution of 4 cm^{-1}. Particle morphology was also examined using field-emission scanning electron microscopy (SEM, Sirion) at 10 kV.

Electrochemical Characterization. The carbon fiber-interwoven amorphous nano-$SiO_{0.37}$/graphene electrode was prepared by casting a slurry of $SiO_{0.37}$/graphene/carbon fiber (75 wt %), carbon black (super-P, 10 wt %) and binder (15 wt %) onto a copper foil. The binder consisted of sodium carboxymethyl cellulose (MW 250,000, Aldrich): PAA (MW 1800, Aldrich) at 1:1 weight ratio in water. The coated electrode was vacuum-dried at 30 °C for 12 h and 110 °C for 12 h. The 2016 coin half-cells, which consisted of carbon fiber-interwoven amorphous $SiO_{0.37}$/graphene or $SiO_{0.37}$/graphene electrode as a working electrode, a lithium foil as a counter electrode, the electrolyte of 1 M $LiPF_6$/fluorinated ethylene carbonate (FEC):diethyl carbonate (DEC) (1:1 volume ratio, Panax E-tech) and separator (Celgard C210), were assembled in Ar-filled glovebox for the evaluation of electrochemical cycling performance. The coin cells of grahene only and carbon fiber only electrodes were also prepared as references to determine their contribution to specific capacities. The coin cells were cycled between 0.05 to 1.5 V at a constant current 300 mAg^{-1} (corresponding to ~C/5 rate)−constant voltage mode, using multichannel cycler (WBCS3000, Wonatech). For the evaluation of rate capability, a lithium cell was charged at various *C* rates of *C*/10 (150 mAg^{-1}), *C*/5 (300 mAg^{-1}), *C*/2 (750 mAg^{-1}), 1C (1.5 Ag^{-1}) and 5*C* (7.5 Ag^{-1}), and discharged at the fixed rate of *C*/10.

RESULTS AND DISCUSSION

Scheme 1 illustrates the RT reduction of amorphous silica into amorphous SiO_x via a simple single displacement of oxygen from silica to lithium metal

$$(4 - 2x)\mathrm{Li} + \mathrm{SiO_2} \rightarrow (2 - x)\mathrm{Li_2O} + \mathrm{SiO}_x \quad (1)$$

followed by composite formation in aqueous solution. Synthesized black SiO_x nanoparticles were added to the PAA-containing RT aqueous suspension of graphene/carbon fibers while conducting ultrasonication till obtaining the suspension of SiO_x/graphene/carbon fiber (Figure 2a). By introducing the surface hydroxyl groups to carbon fibers using acid treatment and by using PAA as a dispersion agent, their dispersion in water significantly improved (Figure 1a, b). Upon lowering pH to 3 of the suspension, which neutralizes the negative charge of oxygen-containing groups at the surface of graphene nanosheets by uptaking protons from acid, agglomeration of graphene nanosheets occur as shown in Figure 2b. This event brings about in situ incorporation of SiO_x nanoparticles and carbon fibers in between graphene nanosheets.

TEM and elemental mapping images of synthesized SiO_x nanoparticles (Figure 3a) reveal a uniform distribution of Si (green) and O (red) atoms over bulk (see scale bar of 200 nm) SiO_x nanoparticles rather than individual particle. Measurements on several spots provide the average chemical formula of $SiO_{0.37}$. Considering that the detection limit of TEM elemental mapping in our measurement condition is in the range of 0.5−3 wt %, the chemical formula is written as $SiO_{0.37\pm0.02}$.

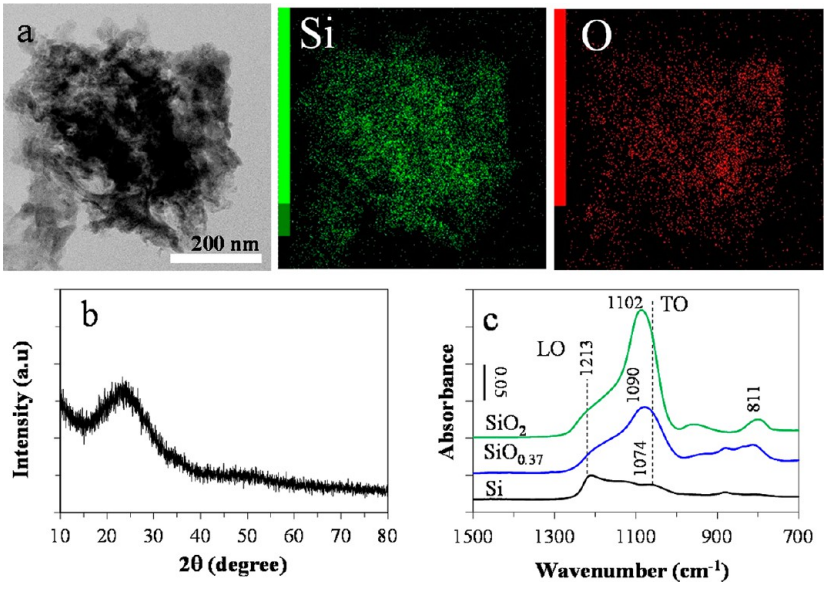

Figure 3. (a) TEM and elemental mapping images and (b) powder XRD pattern of synthesized SiO_{037} nanoparticles, and (c) ATR FTIR spectral comparison of our amorphous SiO_{037} nanoparticles with commercial crystalline nano-Si and nano-SiO_2 powders.

Powder XRD pattern of $SiO_{0.37}$ nanoparticles (Figure 3b) shows a broad feature of reflections, characteristic of amorphous material. Supportive information of composition and local structure of amorphous $SiO_{0.37}$ nanoparticles is obtained from ATR FTIR spectroscopy. Spectral comparison of our $SiO_{0.37}$ to commercial crystalline nano-Si and nano-SiO_2 powders (Figure 3c) shows the red-shift of transverse optical (TO) band of nano-SiO_2 at 1102 cm^{-1}, attributed to ν_{asym} (Si−O) of constituent SiO_4 tetrahedral, to 1090 cm^{-1} of $SiO_{0.37}$ to 1074 cm^{-1} of nano-Si.[7,28] This red-shift is ascribed to the weakening and lengthening of Si−O bond in the order of SiO_2, $SiO_{0.37}$ and Si. Substantial reduction in band absorbance of TO mode and of ν_{sym}(Si−O−Si) at 810 cm^{-1} in the same order is pertained to a decrease in oxygen content.

Figure 4a shows HRTEM image of $SiO_{0.37}$/graphene/carbon fiber. Particle morphology for each component is distinguished and all components appear to be in a close contact with each other. The presence of graphene nanosheets and carbon fibers that surround $SiO_{0.37}$ nanoparticles is advantageous for electrical conductivity. Primary particle size of $SiO_{0.37}$ (Figure 4b) is 20−30 nm in diameter. The absence of lattice fringes on $SiO_{0.37}$ nanoparticles, and dispersed SAED pattern (Figure 4b, inset) confirms that the $SiO_{0.37}$ is amorphous, consistent with XRD data (Figure 3b). Homogeneous distribution of carbon fibers over composite is better observed in SEM images (Figure 4c, d). Carbon fibers are interwoven throughout the secondary particles of 200−300 nm, connecting the SiO_x nanoparticles and graphene nanosheets.

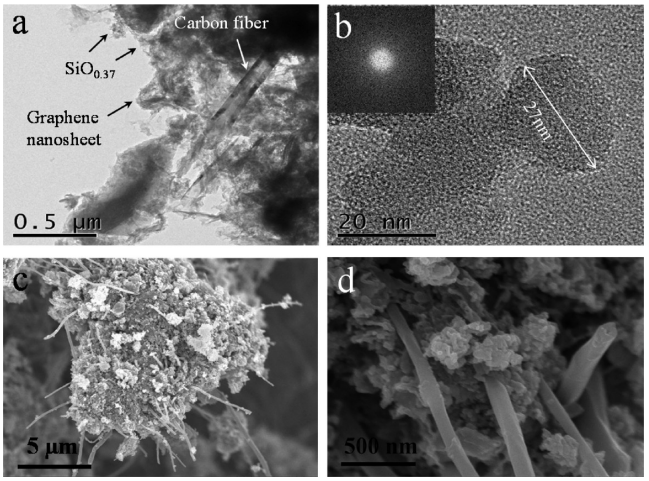

Figure 4. (a) HRTEM images of carbon fiber-interwoven amorphous nano-$SiO_{0.37}$/graphene composite and (b) magnification of $SiO_{0.37}$ nanoparticles and their SAED pattern (inset), and (c, d) SEM images of the composite.

The electrochemical performance of carbon fiber-interwoven amorphous nano-$SiO_{0.37}$/graphene electrode was investigated in lithium cells, which consists of FEC-based electrolyte. FEC is noticed to offer better cycling stability of Si-based anodes than ethylene carbonate (EC)-based electrolytes.[7,29−32] Panels a and b in Figure 5 show charge (lithiation)−discharge (delithiation) voltage profiles and differential capacity plots at C/5 (300 mAg^{-1}) in the voltage range of 0.05−1.5 V. In the differential capacity plots (Figure 5b), a large cathodic peak near 0.3 V during initial charging is due to the formation of Li_2O and lithium silicates and lithiation of amorphous Si, and that at 0.08 V to continued formation of amorphous Li_ySi. In the reverse process, anodic peaks at 0.27 and 0.47 V are by stepwise delithiation of Li_ySi reproducing amorphous Si.[1,2] The anodic peak at 0.47 V is enlarged in the 10th cycle, probably due to the reaction of unused Li_ySi nanoparticles that are isolated in the deep part of bulk or located close to inactive Li_2O and various lithium silicates. This event can occur by inhomogeneous local distribution of different phases (various Li_ySi, Li_2O, various lithium silicates) formed in the early cycles but they are fully utilization in later cycles. Initial charge and discharge capacities are 1965 and 1579 $mAhg^{-1}$ (based on the weight of $SiO_{0.37}$) with Coulombic efficiency of 80%. The total charge and discharge capacities, obtained based on the total weight of $SiO_{0.37}$/graphene/carbon fiber composite, for the initial cycle are 1499 and 1205 $mAhg^{-1}$, as their contents in the $SiO_{0.37}$/

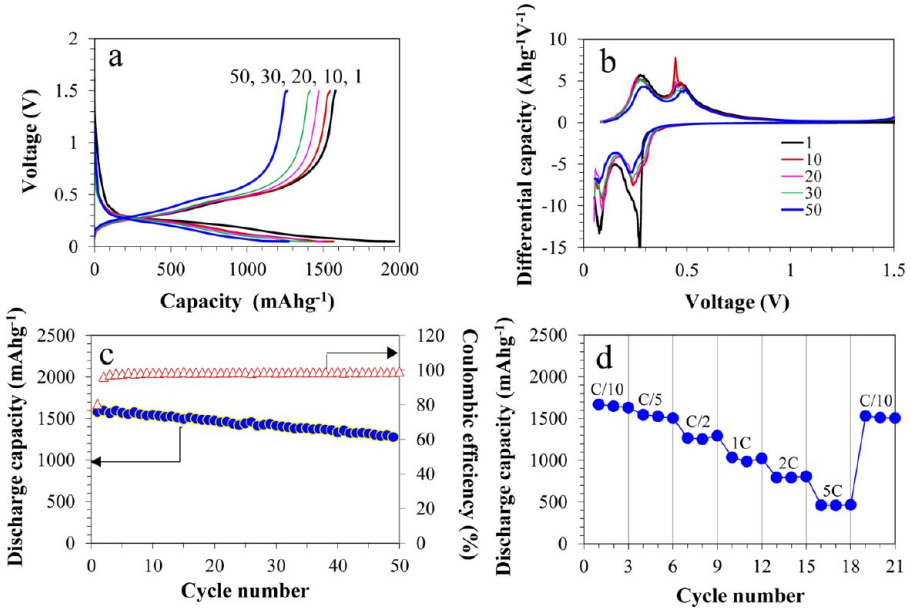

Figure 5. (a) Voltage profiles and (b) differential capacity plots, and (c) discharge capacity and Coulombic efficiency for 50 cycles at the rate of C/5, (d) and high-rate capability up to 5C of the lithium cell with carbon fiber-interwoven amorphous nano-$SiO_{0.37}$/graphene electrode.

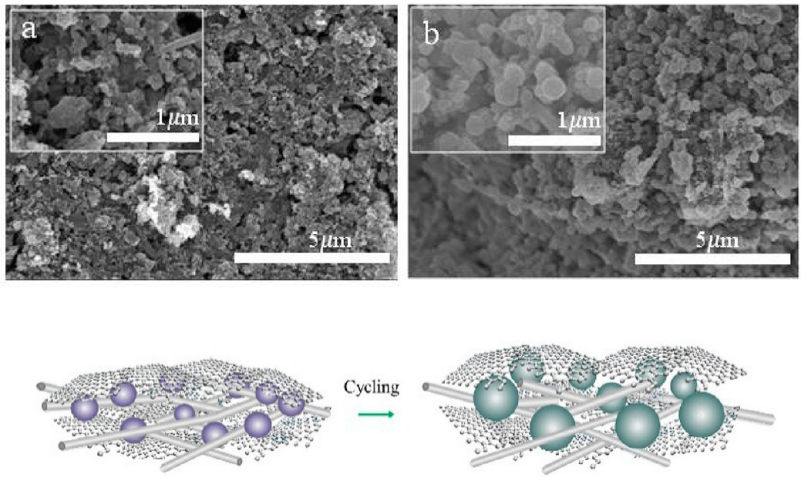

Figure 6. Comparison of SEM images (a) before and (b) after 50 cycles at the rate of *C*/5, and the schematic of flexible and robust microstructure of carbon fiber-interwoven amorphous nano-$SiO_{0.37}$/graphene electrode.

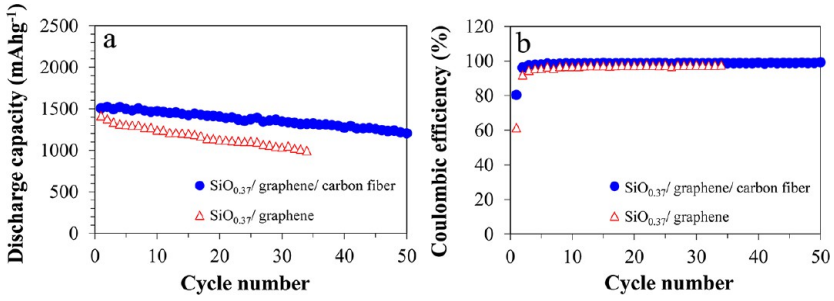

Figure 7. Comparative plots of (a) discharge capacities and (b) Coulombic efficiencies of carbon fiber-interwoven amorphous nano-$SiO_{0.37}$/graphene electrode and amorphous nano-$SiO_{0.37}$/graphene electrode without carbon fiber, cycled at the rate of *C*/5 in the voltage range of 0.05 - 1.5 V.

graphene/carbon fiber composite are each 10 wt %. The contribution of graphene only and carbon fiber only to the initial charge capacity was determined to be small (not shown) as 135 and 42 $mAhg^{-1}$. From the second cycle, their contribution to charge capacities becomes even smaller, similar to that to discharge capacity as 20 and 36 $mAhg^{-1}$, respectively. This implies that the charge and discharge capacities of the composite electrode mainly come from $SiO_{0.37}$. The Coulombic efficiency increases to higher than 97% after 2 cycles. It was reported that irreversible formation of Li_2O and lithium silicates during initial reaction of SiO with lithium resulted in quite a low initial Coulombic efficiency below 65%.[1,2] By lowering the fraction of oxygen and having graphene/carbon fiber, our electrode enables to improve initial Coulombic efficiency to 80%. As revealed in differential capacity plots (Figure 5b), maintained structural resolution of the prominent peaks with lithiation and delithiation over 50 cycles is indicative of high cycling reversibility and ability. The electrode exhibits impressive cycling performance with capacity retention of 80% of the initial discharge capacity at the 50th cycle, delivering discharge capacities of 1579−1263 $mAhg^{-1}$ and well-maintained Coulombic efficiencies of 99%.

Excellent rate-capability up to 5C (7.5 Ag^{-1}) is achieved on the electrode as displayed in Figure 5d. At a 5*C* rate, discharge capacity is 561 $mAhg^{-1}$, still larger than the theoretical capacity (372 $mAhg^{-1}$) of graphite. This high-rate performance is ascribed to a unique microstructure and composition; synergetic effects of the open spaces between graphene nanosheets formed by carbon fiber pillars, homogeneously dispersed three components, amorphous $SiO_{0.37}$ nanoparticles and enhanced conductivity by the presence of graphene and carbon fiber allow an accommodation of volume change of Li_ySi, and offer microstructural robustness and promoted kinetics of lithium-diffusion and electron transport.

Images a and b in Figure 6 show the particle morphology before and after cycling of carbon fiber-interwoven amorphous nano-$SiO_{0.37}$/graphene electrode at a rate of *C*/5. The microstructure of the electrode after cycling (Figure 6b) is nearly sustained, compared to that of pristine electrode (Figure 6a), implying its microstructural robustness. With cycling the particle size of $SiO_{0.37}$ apparently enlarges to 100−120 nm (Figure 6b) in diameter, probably due to remained volume expansion and/or aggregation of primary particles. Nevertheless, flexible characteristic of graphene nanosheets and the open spaces formed by interweaving carbon fibers in between graphene nanosheets might accommodate the volume change and sustain the microstructure as illustrated in the scheme in Figure 6.

In the absence of carbon fiber (i.e., SiO_x/graphene only composite), the electrode shows a relatively rapid capacity fade with low initial efficiency of 62% (Figure 7). This demonstrates the effective role of interweaving carbon fibers throughout the secondary $SiO_{0.37}$/graphene particles in connecting the $SiO_{0.37}$ nanoparticles and graphene nanosheets. It is thus determined that carbon fiber contributes to maintaining the microstructure

and particles connectivity, and high cycling stability and rate-performance.

CONCLUSIONS

Successful room temperature facile syntheses of amorphous SiO_x nanoparticles and highly dispersed carbon fiber-interwoven amorphous nano-$SiO_{0.37}$/graphene in aqueous solution, and its evaluation as a battery anode are reported. The carbon fiber-interwoven amorphous nano-$SiO_{0.37}$/graphene electrode exhibits impressive cycling performance and sustained microstructure after cycling, and high-rate performance up to 5*C*. This demonstrates that the combinative effectiveness of amorphous SiO_x nanoparticles with low fraction of oxygen, homogeneously dispersed three components, unique microstructure including the open spaces between graphene nanosheets formed by carbon fiber pillars, and improved electrical conductivity by the presence of graphene and carbon fibers offers the accommodation of volume change, the microstructural robustness and flexibility, promoted kinetics of lithium-diffusion and electron transport, leading to improved cycling performance. The use of appropriate electrolyte component, which has a high interfacial compatibility with the electrode, contributes to further improvement of the cycling performance. We believe that our materials design and synthesis provide a useful platform for scalable preparation of various nonstoichiometric suboxide- and graphene-based composite electrode materials.

AUTHOR INFORMATION

Corresponding Author

*E-mail: swsong@cnu.ac.kr. Phone: +82-42-821-7008. Fax: +82-42-822-6637.

Notes

The authors declare no competing financial interest.

ACKNOWLEDGMENTS

This work was supported partly by the Korean Ministry of Education and National Research Foundation through the Human Resource Training Project for Regional Innovation (2012026203) and partly by the Converging Research Center Program (2013K000214) through the Ministry of Science, ICT & Future Planning.

REFERENCES

(1) Obrovac, M. N.; Krause, L. J. *J. Electrochem. Soc.* **2007**, *154*, A103−A108.
(2) Yang, J.; Takeda, Y.; Imanishi, N.; Capiglia, C.; Xie, J. Y.; Yamamoto, O. *Solid State Ionics* **2002**, *153*, 125−129.
(3) Nagao, Y.; Sakaguchi, H.; Honda, H.; Fukunaga, T.; Esaka, T. *J. Electrochem. Soc.* **2004**, *151*, A1572−A1575.
(4) Doh, C. H.; Park, C. W.; Shin, H. M.; Kim, D. H.; Chung, Y. D.; Moon, S. I.; Jin, B. S.; Kim, H. S.; Veluchamy, A. *J. Power Sources* **2008**, *179*, 367−370.
(5) Kim, K.; Park, J.-H.; Doo, S.-G.; Kim, T. *Thin Solid Films* **2010**, *518*, 6547−6549.
(6) Abel, P. R.; Lin, Y.-M.; Celio, H.; Heller, A.; Mullins, C. B. *ACS Nano* **2012**, *6*, 2506−2516.
(7) Nguyen, C. C.; Choi, H.; Song, S.-W. *J. Electrochem. Soc.* **2013**, *160*, A906−A914.
(8) Beaulieu, L. Y.; Hewitt, K. C.; Turner, R. L.; Bonakdarpour, A.; Abdo, A. A.; Christensen, L.; Eberman, K. W.; Krause, L. J.; Dahn, J. R. *J. Electrochem. Soc.* **2003**, *150*, A149−A156.
(9) Wang, C. S.; Wu, G. T.; Zhang, X. B.; Qi, Z. F.; Li., W. Z. *J. Electrochem. Soc.* **1998**, *145*, 2751−2758.
(10) Hu, Y.-S.; Demir-Cakan, R.; Titirici, M.-M.; Müller, J.-O.; Schlögl, R.; Antonietti, M.; Maier, J. *Angew. Chem., Int. Ed.* **2008**, *47*, 1645−1649.
(11) Magasinski, A.; Dixon, P.; Hertzberg, B.; Kvit, A.; Ayala, J.; Yushin, G. *Nat. Mater.* **2010**, *9*, 353−358.
(12) Ng, S.-H.; Wang, J.; Wexler, D.; Konstantinov, K.; Guo, Z.-P.; Liu, H.-K. *Angew. Chem., Int. Ed.* **2006**, *45*, 6896−6899.
(13) Wang, J.; Zhaoa, H.; He, J.; Wang, C.; Wang, J. *J. Power Sources* **2011**, *196*, 4811−4815.
(14) Baggetto, L.; Danilov, D.; Notten, P. H. L. *Adv. Mater.* **2011**, *23*, 1563−1566.
(15) Ma, H.; Cheng, F.; Chen, J.-Y.; Zhao, J.-Z.; Li, C.-S.; Tao, Z.-L.; Liang, J. *Adv. Mater.* **2007**, *19*, 4067−4070.
(16) Yu, Y.; Gu, L.; Zhu, C.; Tsukimoto, S.; van Aken, P. A.; Maier, J. *Adv. Mater.* **2010**, *22*, 2247−2250.
(17) Heath, J. R. *Science* **1992**, *258*, 1131−1133.
(18) Kim, H.; Seo, M.; Park, M.-H.; Cho, J. *Angew. Chem., Int. Ed.* **2010**, *49*, 2146−2149.
(19) Bao, Z.; Weatherspoon, M. R.; Shian, S.; Cai, Y.; Graham, P. D.; Allan, S. M.; Ahmad, G.; Dickerson, M. B.; Church, B. C.; Kang, Z.; Abernathy, H. W.; Summers, C. J.; Liu, M.; Sandhage, K. H. *Nature* **2007**, *446*, 172−175.
(20) Yang, X.; Wen, Z.; Xu, X.; Lin, B.; Huang, S. *J. Power Sources* **2007**, *164*, 880−884.
(21) Lee, J. K.; Smith, K. B.; Hayner, C. M.; Kung, H. H. *Chem. Commun.* **2010**, *46*, 2025−2027.
(22) He, Y.-S.; Gao, P.; Chen, J.; Yang, X.; Liao, X.-Z.; Yang, J.; Ma, Z.-F. *RSC Adv.* **2011**, *1*, 958−960.
(23) Evanoff, K.; Magasinski, A.; Yang, J.; Yushin, G. *Adv. Energy. Mater* **2011**, *1*, 495−498.
(24) Guo, C.; Wang, D.; Wang, Q.; Wang, B.; Liu, T. *Int. J. Electrochem. Sci.* **2012**, *7*, 8745−8752.
(25) Ros, T. G.; van Dillen, A. J.; Geus, J. W.; Koningsberger, D. C. *Chem.—Eur. J.* **2002**, *8*, 1151−1162.
(26) Hummers, W. S.; Offeman, R. E. *J. Am. Chem. Soc.* **1958**, *80*, 1339−1339.
(27) Li, D.; Müller, M. B.; Gilje, S.; Kaner, R. B.; Wallace, G. G. *Nat. Nanotechnol.* **2008**, *3*, 101−105.
(28) Queeney, K. T.; Weldon, M. K.; Chang, J. P.; Chabal, Y. J.; Gurevich, a. B.; Sapjeta, J.; Opila, R. L. *J. Appl. Phys.* **2000**, *87*, 1322−1330.
(29) Nakai, H.; Kubota, T.; Kita, A.; Kawashima, A. *J. Electrochem. Soc.* **2011**, *158*, A798−A801.
(30) Lin, Y.-M.; Klavetter, K. C.; Abel, P. R.; Davy, N. C.; Snider, J. L.; Heller, A.; Mullins, C. B. *Chem. Commun.* **2012**, *48*, 7268−7270.
(31) Song, S.-W.; Baek, S.-W. *Electrochem. Solid-State Lett.* **2009**, *12*, A23−A27.
(32) Nguyen, C. C.; Song, S.-W. *Electrochim. Acta* **2010**, *55*, 3026−3033.